Effect of Alclad Layer on Material Flow and Defect Formation in Friction-Stir-Welded 2024 Aluminum Alloy

Z. ZHANG, B.L. XIAO, D. WANG, and Z.Y. MA

The effect of the Alclad layer on material flow and defect formation during friction-stir welding (FSW) of 6.5-mm-thick 2024Al-T351 alloy plates was investigated. To characterize the material flow during FSW, different cross sections of the keyhole and "stop-action weld" were made for metallographic observations. It was found that the top Alclad assembled at the shoulder/workpiece interface, thereby weakening the material flow in the shoulder-driven zone and favoring the formation of void defect at high traveling speeds. The bottom Alclad layer extended into the weld at excess material flow state, which could be avoided at balanced material flow state. A conceptual model of material flow was proposed to describe the formation of the weld. It was indicated that a perfect FSW joint of Alclad 2024Al alloy without defect could be obtained at an optimum FSW condition.

DOI: 10.1007/s11661-010-0545-3

I. INTRODUCTION

A typical high-strength aluminum alloy, 2024 aluminum (2024Al) alloy is gaining commercial importance in aerospace industries as wing and fuselage structures where high specific strength and fatigue resistance are required.[1] It is usually clad with pure aluminum or Al-1Zn alloy to improve the corrosion resistance. However, its industrial application is restricted by the process technology, especially welding technology, because it is unweldable using the conventional fusion welding techniques because of its hot cracking sensitivity. The structures are fastened together usually using rivets that not only increase the weight but also reduce the fatigue properties.[2] Therefore, a new welding method that can join the high-strength aluminum alloys is highly desirable.

Friction-stir welding (FSW), which is a relatively new solid-state joining process that uses a nonconsumable rotating welding tool to generate frictional heat at the welding location without material melting, produces pore-free joints and smaller temperature gradient than conventional arc processes.[3,4] Consequently, FSW is considered an ideal process for joining high-strength aerospace aluminum alloys that typically are difficult to weld.[5]

In the previous studies,[5–7] Unclad 2024Al plates were subjected to extensive FSW investigations, and it was reported that the Unclad 2024Al plates could be welded successfully by FSW. However, the FSW of an Alclad 2024Al alloy was seldom conducted.[8] Talwar *et al.*[8] reported that the Alclad layer on the root surface of the weld was brought into the interior of the weld along the advancing boundary of the nugget zone (NZ) and thermomechanically affected zone (TMAZ), which deteriorated the mechanical properties of the weld. Machining the root side to remove the Alclad layer increased the ductility and tensile strength of the weld. However, the effect of the top Alclad layer was not mentioned in their research. It should be pointed out that for the engineering applications, it is not a wise method to remove the surface layer by machining. Thus, the FSW of the Alclad 2024Al alloy becomes of practical significance.

During FSW, heat is generated by the friction between the welding tool and the workpiece, and by the plastic deformation around the tool, which determines the weld microstructure and properties.[3] Thus, the tool/workpiece interface plays an important role during FSW. Reynolds[9] reported that the condition of the tool/workpiece interface affected the material flow strongly, but they did not give the details. For FSW of the Alclad 2024Al alloy, the Alclad layer may change the tool/workpiece interface condition. Therefore, it is worthwhile to investigate the effect of the Alclad layer on the FSW process of 2024Al alloy for both engineering application and scientific analysis.

A series of investigations has discussed the material flow during FSW. As the material flow could not be observed directly, a specific marker material was used to mark the material flow path in the previous literature. Several kinds of materials, such as steel shots 0.38 mm in diameter,[10] aluminum alloy sheet,[11] pure aluminum sheet,[12] and pure copper foil,[13,14] were inserted at the different locations of the faying surface to trace the material flow. Based on the distribution of the marker material in the weld, some important information about the material flow during FSW was revealed.[10–14] However, the inserted marker material might change the state of the faying face. Thus, the real material flow may not be represented properly.

Z. ZHANG, Postgraduate, B.L. XIAO, Professor, D. WANG, Assistant Professor, and Z.Y. MA, Professor, are with the Shenyang National Laboratory for Materials Science, Institute of Metal Research, Chinese Academy of Sciences, Shenyang 110016, P.R. China. Contact e-mail: zyma@imr.ac.cn
Manuscript submitted April 27, 2010.
Article published online November 24, 2010

Recently, the effect of welding tools[15–17] and welding parameters[18] on the material flow was studied, revealing the general material flow features during FSW. The shoulder drove the material to form a shoulder-driven zone in the upper region of the workpiece. In the lower region, the pin drove the material to form a pin-driven zone. The material flew from the top to the lower part, from the front side to the trailing side. Furthermore, these studies also revealed the intricate relationships between tool geometry, FSW parameters, defect formation, onion ring structure, and material flow.[15–18] However, experimental observations could not elucidate the overall issues; the material flow models are needed to understand the whole flow process. Schmidt and Hattel[19] proposed a numerical computational fluid dynamics model to predict the material flow around the pin. Arbegast[20] proposed a mass-balanced flow model to address the relation of the defect formation to the mass and direction of the flowing material.

Despite these important aspects, some controversies concerning the flow paths still exist. Furthermore, no model addressed the material flow details during the whole FSW process. For the Alclad 2024Al alloy, the inherent Alclad layer is a good mark material for FSW, which may help to clarify the controversies by tracing the material flow. In this work, the effects of the Alclad layer on the material flow and defect formation during FSW were studied. To observe the real material flow, the stirring pin was "frozen" in the workpiece by making the pin naturally break during FSW to produce a "stop action" weld. A conceptual model of the FSW process is proposed to increase the understanding of material flow mechanism and illustrate the role of the Alclad layer during FSW.

II. EXPERIMENTAL PROCEDURE

The materials used in this study are a 6.5-mm-thick Alclad 2024Al-T351 rolled plate and 5.0-mm-thick Unclad 2024Al-T351 rolled plate, which was produced by removing the double side Alclads of Alclad 2024Al-T351. The plates with a length of 400 mm and a width of 70 mm were butt welded along the rolling direction with a tool tilt angle of 2.7 deg using an FSW machine (China FSW Center, Beijing, China). A tool with a shoulder 20 mm in diameter and a threaded cylindrical pin 8 mm in diameter was used. To understand the effect of the Alclad layer on the material flow, the Alclad and Unclad 2024Al-T351 plates were welded in different FSW parameters, which are shown in Table I. To facilitate the comparison, we define the commonly applied plunge depth of 0.2 to 0.5 mm and the rarely used plunge depth of >0.5 mm as the small plunge depth (SD) and large plunge depth (LD), respectively. It should be pointed out that the plunge depth in this study is the nominal value displayed on the machine, which is different from the effective plunge depth defined as the depth of the lowest point of the shoulder below the surface of the welded plate. The FSW samples were designated in brief forms. For example, the Alclad sample represents the FSW weld of the Alclad 2024Al-T351; Alclad sample SD-800-100 denotes the Alclad plate welded at a rotation rate of 800 rpm and a traveling speed of 100 mm/min under a small plunge depth.

Table I. Welding Parameters of FSW 2024Al–T351 Joints

Sample	Rotation Rate ω (rpm)	Traveling Speed v (mm/min)	Plunge Depth (mm)	Designation
Alclad sample	800	100	0.2 to 0.5	SD-800-100
	800	200	0.2 to 0.5	SD-800-200
	800	400	0.2 to 0.5	SD-800-400
	800	200	>0.5	LD-800-200
	800	400	>0.5	LD-800-400
Unclad sample	800	100	0.2 to 0.5	SD-800-100
	800	200	0.2 to 0.5	SD-800-200
	800	400	0.2 to 0.5	SD-800-400

To observe the "stop-action" sample, we made the pin comparatively harder and more brittle by heat treatment as mentioned in Reference 21. In this way, the pin would break during FSW and be embedded in the workpiece, making it possible to observe the real material flow pattern during FSW.

All the samples used for the metallographic analyses were cross sectioned from the joints perpendicular to the welding direction using an electrical discharge machine (DK7732, Kedi CNC Machinery Co., Ltd, Taizhou, China). After grinding and polishing, the samples were etched using Keller's reagent (190 mL water, 3 mL nitric acid, 2 mL hydrochloric acid, and 5 mL hydrologic acid) and observed through an optical microscope (OM; HC-300Z/OL, Olympus Corporation, Tokyo, Japan).

III. RESULTS

A. *Types of Defect in FSW Joints*

Figure 1 shows the macrographs of the cross sections and upper surfaces of the FSW 2024Al-T351 joints under different welding parameters. It can be observed that the FSW Alclad and Unclad 2024Al-T351 joints exhibited different microstructures and surface qualities. In this case, we are interested mainly in the structural features of the Alclad samples and the differences between Alclad and Unclad samples. The main results are described as follows.

For the cross sections of the Alclad samples (Figures 1(a) through (e)), the white zones at the top and bottom of the welds were the Al layer, *i.e.*, the residual Alclad layer. The zones marked with the white boxes contained the void defects. Under the small plunge depth, no void was detected in the low-traveling-speed (100 mm/min) weld, but the bottom surface Alclad layer was brought into the interior of the weld along the boundaries of the NZ at both the advancing and retreating sides (Figure 1(a)). At a higher traveling speed of 200 mm/min, the voids appeared and enlarged with increasing the traveling speed to 400 mm/min (Figures 1(b) and (c)). Increasing the plunge depth led to the void disappearance in the welds prepared at both traveling speeds of 200 and 400 mm/min (Figures 1(d) and (e)).

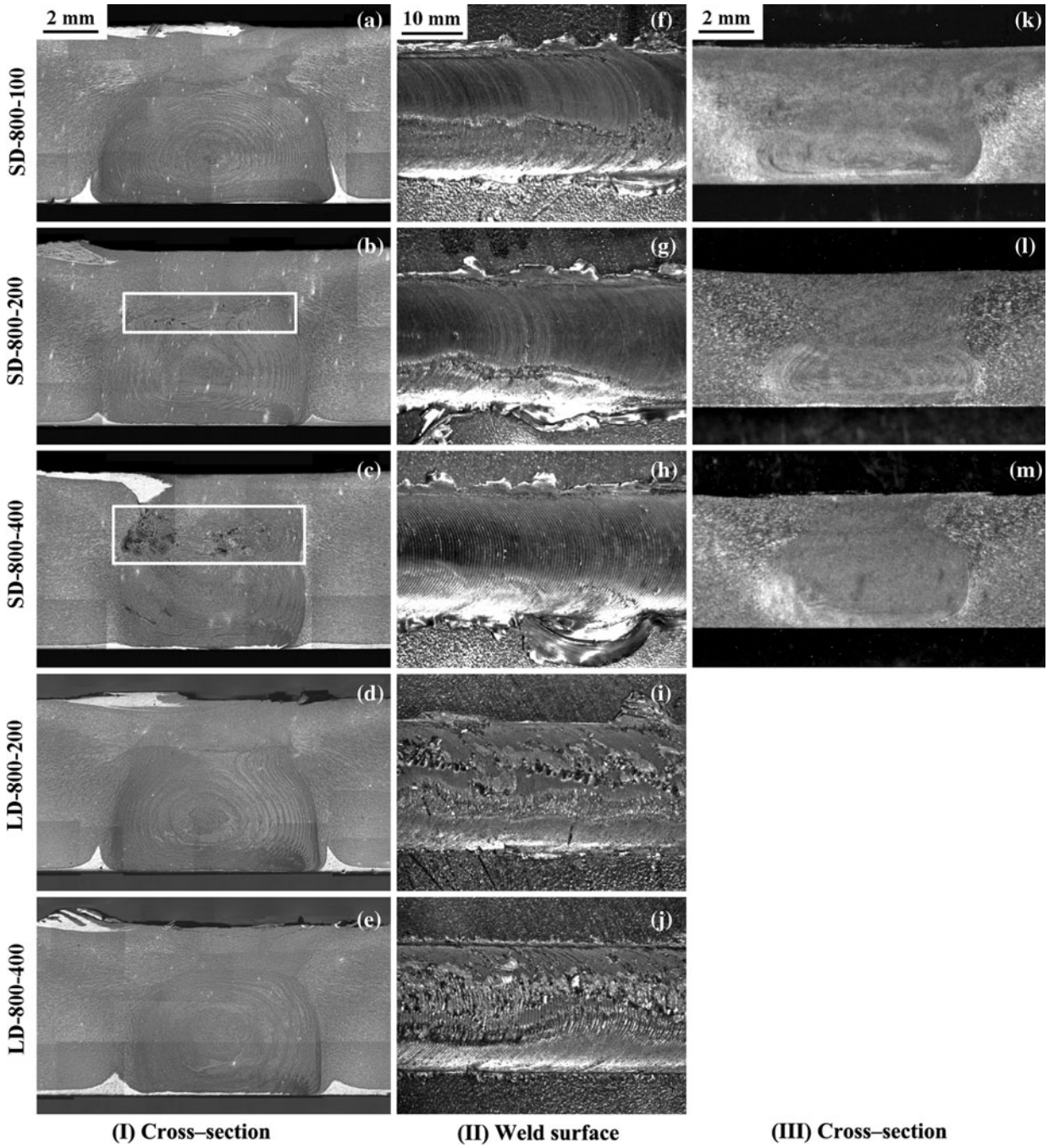

Fig. 1—Macrographs of cross sections and upper surfaces of (I) and (II) Alclad samples and (III) Unclad samples under different traveling speeds and plunge depths.

For the superficial aspect of the Alclad samples (Figures 1(f) through (j)), the convex parts on the top surfaces of the joints were the Al layer corresponding to the white zones of the cross-sectional macrographs. The surface of the welds with a small plunge depth was smoother than that with a large plunge depth, which indicates that the weld surface quality was controlled mainly by the plunge depth.

For the Unclad samples, sound welds were obtained at all the traveling speeds ranging from 100 to 400 mm/min under small plunge depth (Figures 1(k) through (m)). These results are different from those for the Alclad samples under the same plunge depth (Figures 1(a) through (c)), where the high traveling speeds led to the formation of the void defects.

B. *The Role of Alclad Layer During FSW*

To clarify the effect of the Alclad layer on the material flow during FSW, the cross sections of the keyhole of the Alclad and Unclad samples were observed by OM. Figure 2 shows the macroscopic

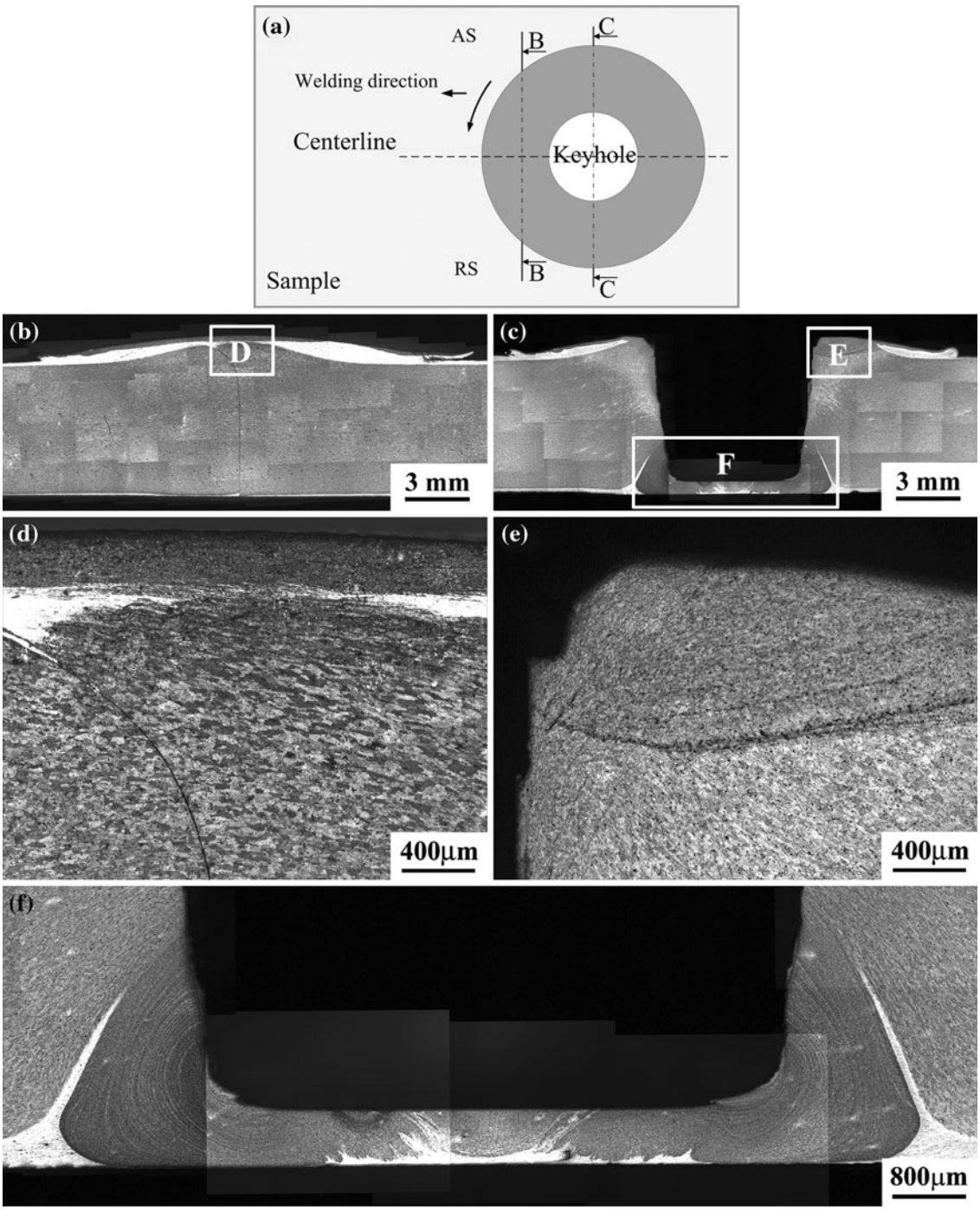

Fig. 2—Transverse cross sections of keyhole of Alclad sample SD-800-100: (*a*) top schematic views of position of various cross sections in keyhole; (*b*) section B-B; (*c*) midsection C-C; (*d*) through (*f*) magnified microstructures of positions D, E, and F as shown in Figs. 2(b) and (c).

views of different sections of the keyhole of Alclad sample SD-800-100. Figure 2(a) shows the position of the cross sections in the keyhole. Figures 2(b) and (c) show that the Alclad layer aggregated at the interface between shoulder and base material. The thickness of the Alclad layer beneath the shoulder was nearly 0.5 mm, which is much thicker than that of the original clad layer of 0.2 mm. It can be observed from Figure 2(b) that the butting line deviated left (the retreating side) and a small highly deformed zone (marked by a white box D), characterized by dynamic recrystallization zone (as shown by a magnified view in Figure 2(d)), formed at the top of the sample. The material close to the pin suffered severe deformation and flowed with the shoulder, and thus the Alclad mixed in this zone (Figure 2(d)). It can be observed from Figure 2(c) that tiny highly deformed zones formed at the top and bottom zones (marked by white

boxes E and F with magnified views being shown in Figures 2(e) and (f), respectively), which were named the shoulder-driven flow zone and the pin-driven flow zone by Kumar and Kailas,[22] respectively.

The macroscopic view of the mid-transverse cross section of the keyhole of Unclad sample SD-800-100 is shown in Figure 3. It can be observed that the shoulder-driven zone connected with the pin-driven zone to form a large highly deformed zone (marked by the black dotted line), which is much larger than that for Alclad sample SD-800-100.

In this study, the stirring tool *in situ* rotated for 2 seconds before it was pulled out of the samples; thus, the keyholes of the Alclad and Unclad samples were obtained under the same welding parameters. The microstructure around the keyhole reflected the material flow characteristics during FSW. The difference in the sizes of the shoulder-driven zone and the pin-driven zone for the Alclad and Unclad samples indicated that the material flow patterns around the tools were distinctly different. Furthermore, this difference indicated that the top Alclad layer exerted a significant effect on the material flow during FSW. The difference in the material flow pattern features of different samples were verified by the comparison of the Alclad and Unclad samples under three welding parameters, as shown in Figure 4.

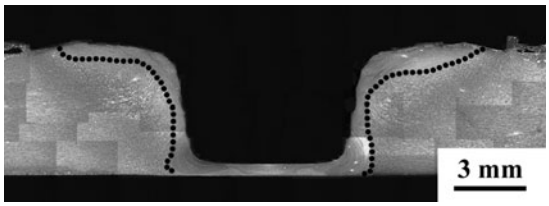

Fig. 3—Mid-transverse cross section of keyhole of Unclad sample SD-800-100.

C. *The Material Flow During FSW*

To understand clearly the material flow process during FSW of the Alclad samples, the transverse cross sections of the SD-800-400 "stop-action" weld of Alclad sample SD-800-400 were observed. Figure 5(a) shows the position of the cross sections in the "stop-action" weld. Figures 5(b) through (d) show the macroscopic views of the three different cross sections: B-B, C-C, and D-D, as shown in Figure 5(a). The representative material flow details around the pin at different positions (positions A, B, and C in Figure 5(b)) are shown in Figure 6.

Figure 5(b) shows the middle section B-B. In this position, the material moved closely with the pin. The material flow direction could be predicted according to the direction of elongated base grains near the NZ. The downward flow of the grains in the TMAZ close to the pin shear zone (Figures 6(a) and (b)) indicated that the material flowed downward in the vertical direction on both advancing and retreating sides of the pin. It can be noticed that a vertical swirl moment occurred beneath the pin and the bottom Alclad layer was mixed into the base 2024Al alloy (Figure 6(c)). No extended Alclad layer was observed. This result suggests that the Alclad layer did not tend to extend into the interior of the weld prepared at a high traveling speed and a small plunge depth.

As shown in Figures 5(c) and (d), at the trailing side, the pin shear layer detached with the pin left a hole at

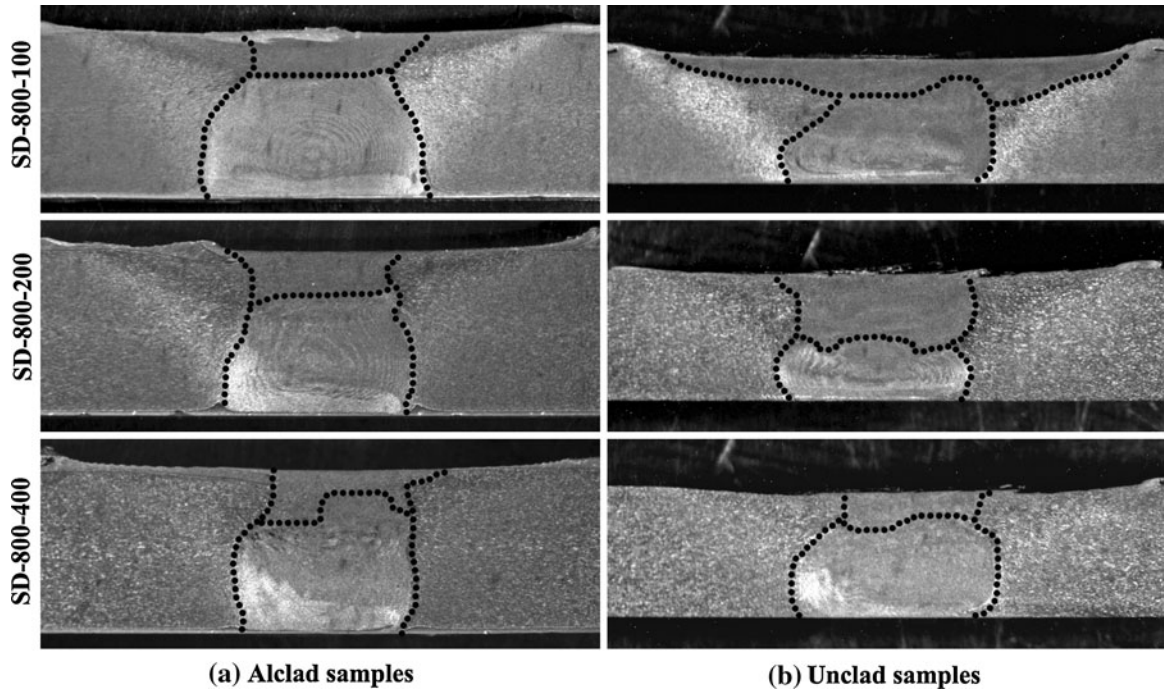

Fig. 4—Characteristics of shoulder-driven and pin-driven zones of (*a*) Alclad samples and (*b*) Unclad samples.

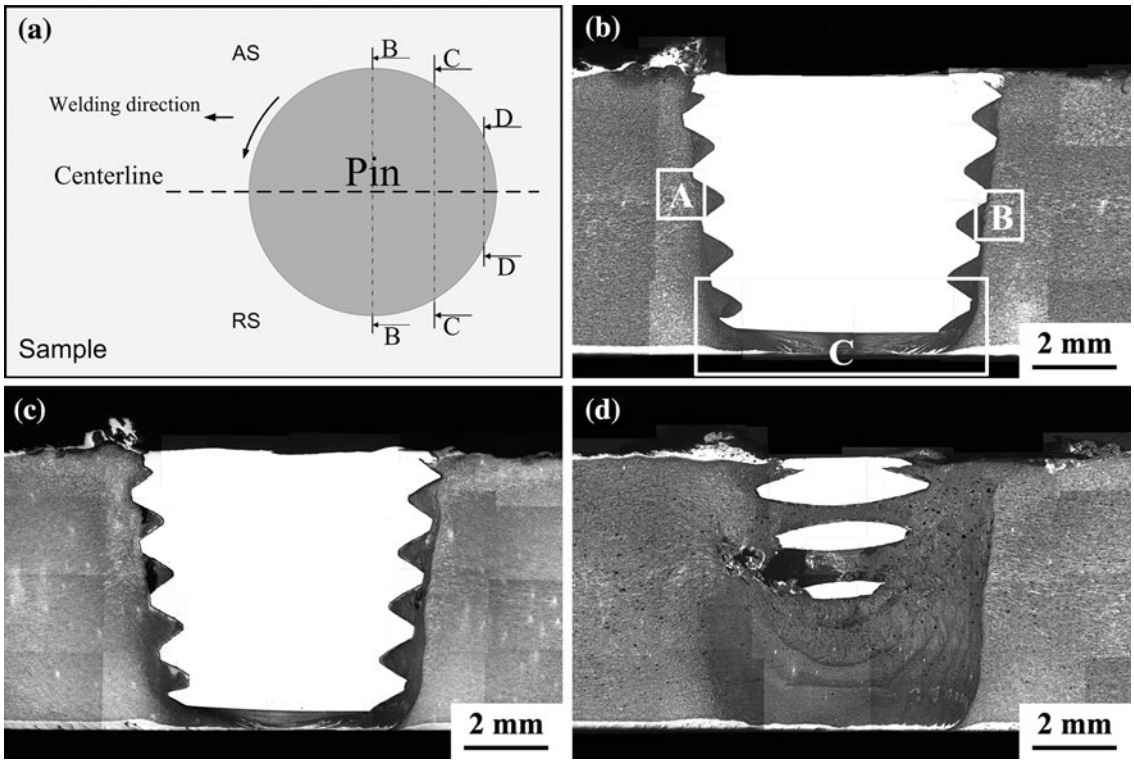

Fig. 5—Transverse cross section of SD-800-400 "stop-action" weld with broken pin embedded: (*a*) top schematic views of position of various cross sections in "stop-action weld," (*b*) midsection B-B, (*c*) section C-C, and (*d*) section D-D.

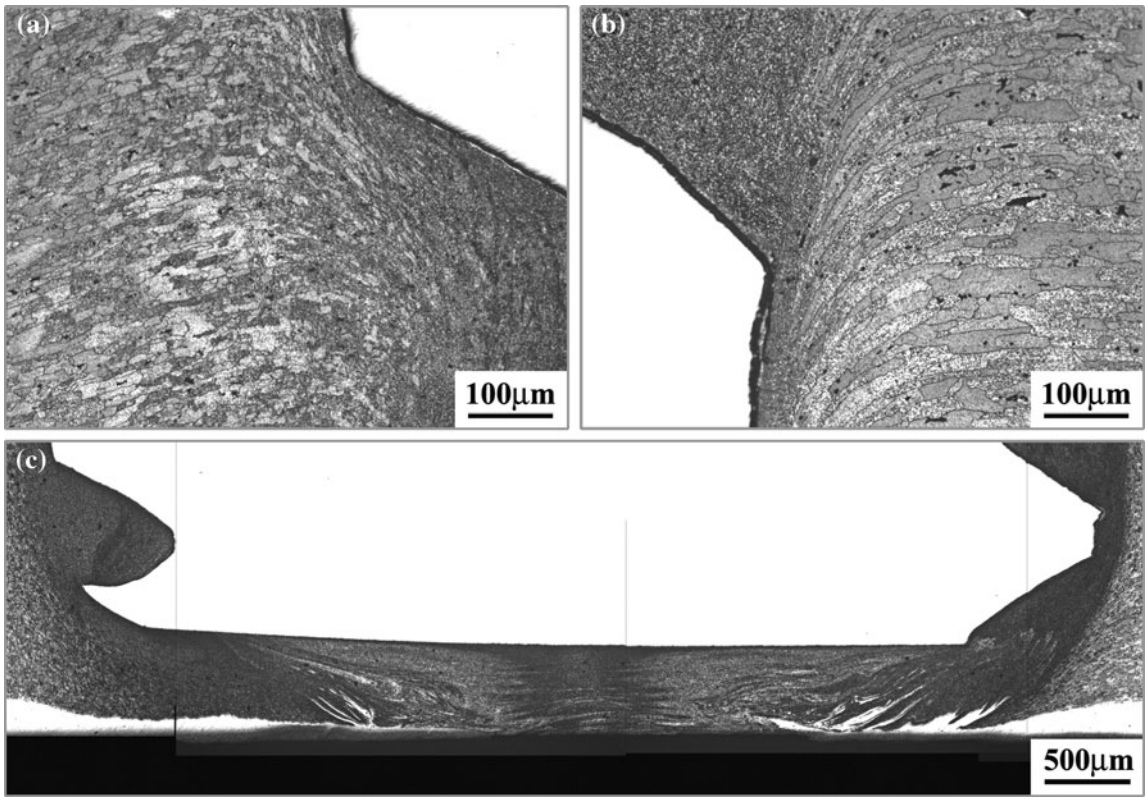

Fig. 6—Magnified micrographs of Fig. 5(b) from position A to position C: (*a*) position A, (*b*) position B, and (*c*) position C.

the back of the pin. At section C-C, the material flow characteristic was similar to that at section B-B. At section D-D, the detached shear layers deposited and formed an initial onion ring structure. The detached shear layers would continue slowly moving upward to fill the hole, pushed by the incoming material.[21] It is noticed that the base material around the hole was forged into the hole at the retreating side, which suggests that the hole was displaced by the upward pin shear material and downward shoulder shear material. Thus, the junction of the shoulder-driven zone and the pin-driven zone is the area most vulnerable to defects.

IV. DISCUSSION

Based on the observations of the macrostructure and material flow, it is clear that the Alclad layer affected the quality of the FSW joints strongly. To explain the role of the Alclad layer and the material flow behavior during FSW of the Alclad 2024Al alloy, based on the experimental investigations presented in this work, the CFD flow model,[19] and the mass balanced flow model,[20] a conceptual model relating the material flow and surface condition is proposed, as shown in Figures 7 and 8.

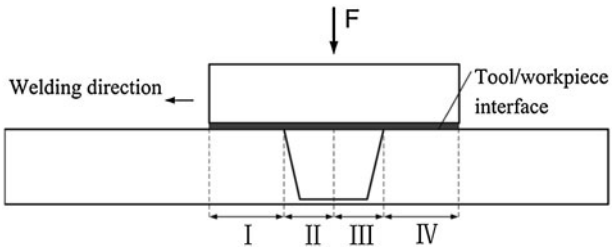

Fig. 7—Schematic diagram for weld formation during FSW.

During FSW of the Alclad samples, the top Alclad layer aggregates at the tool/workpiece interface (Figure 7), which is obviously different from that for the Unclad samples. The change in the tool/workpiece interface would alter the material flow during FSW. To facilitate the understanding of the material flow, the conceptional process of FSW formation can be divided into four main stages, *i.e.*, I, II, III, and IV (Figure 8).

- Stage I can be named the advance deformation process (Figure 8(a)). The material in front of the pin is extruded upward into the conical cavity of the shoulder and closely contacts with the shoulder.[14] The shoulder drives the material to form a shoulder-driven zone. There is no pin-driven material flow zone at this stage. The material around the pin outline suffers slightly plastic deformation.
- Stage II can be named the extrusion process (Figure 8(b)), where the material flows from the leading side to the trailing side on both the advancing and retreating sides of the pin. The pin drives the material to form a shear layer (pin-driven zone). Simultaneously, some material passes beneath the pin from the front to the back to form a swirl zone (SWZ). At this stage, the material flows downward

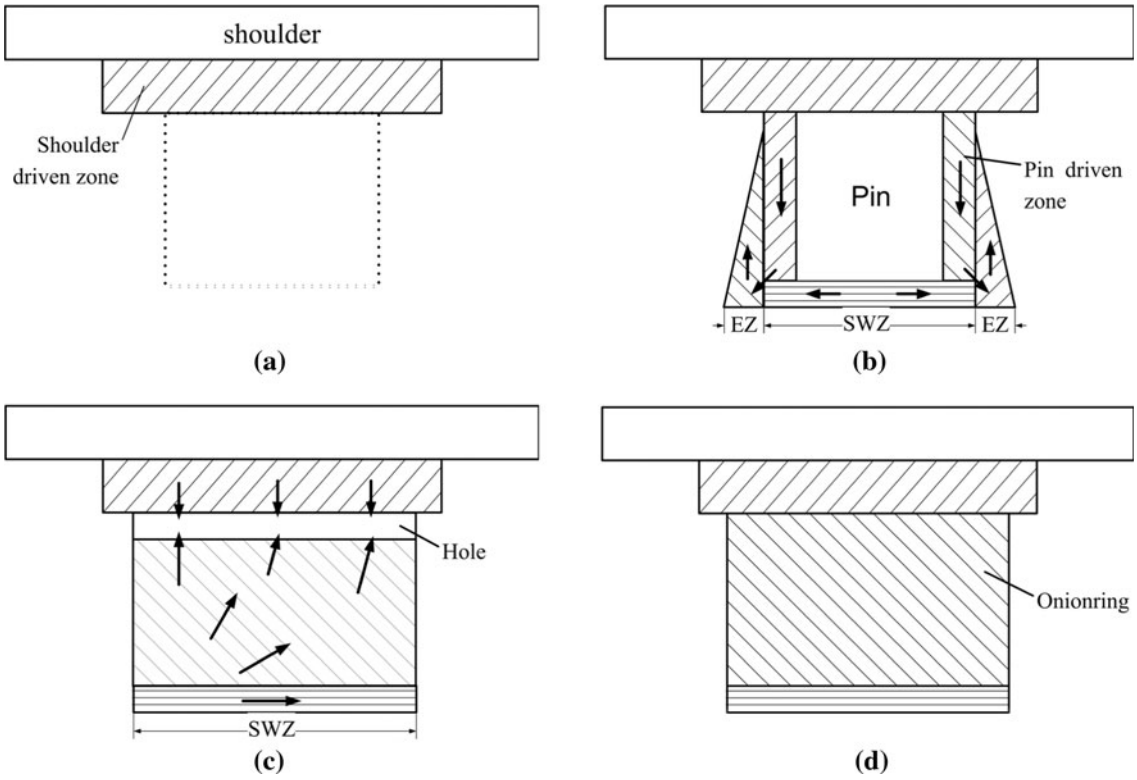

Fig. 8—Conceptual diagrams of different stages of weld formation as shown in Fig. 7: (*a*) stage I, (*b*) stage II, (*c*) stage III, and (*d*) stage IV.

from the upper zone (shoulder-driven zone) to the lower region (pin-driven zone) along the screw thread of the pin. If there is excess material, the material flows outward and upward at the bottom to form an excess material zone (EZ), which enlarges the pin-driven zone.

- Stage III is referred to as the deposition process (Figure 8(c)). At this stage, the shear layer detaches with the pin, leaving a hole at the trailing side of the pin. The deposited layers form the initial nugget zone. The shoulder and pin shear material flows to fill the hole. Insufficient material flow induced by the welding parameters or surface condition will produce a void at the junction zone.
- Stage IV is the formation of the weld surface (Figure 8(d)). In this process, the material in the cavity of the conical shoulder is forged downward to form the weld surface by the shoulder.

Generally speaking, the FSW process is composed of countless material flow cycles. The material moved from the front to the tailing side per cycle. The mass of flowing material per cycle (M^{PC}) was equivalent to the mass of material through the shoulder-driven zone (M^{S}), pin-driven zone (M^{P}), excess zone (M^{EZ}), and swirl zone (M^{SW}) during the extrusion process at stage II, which can be represented by

$$M^{PC} = M^{S} + M^{P} + M^{SW} + M^{EX} \quad [1]$$

It was noted that there is a critical total mass of material (M^{CR}) per cycle for a steady FSW process to the tailing side to avoid the void defects. For the FSW process, the M^{CR} is associated with the rotation rate (ω), the traveling speed (v), and the shapes and sizes of the shoulder and pin, which was originally defined in Reference 20

$$M^{CR} = \rho(\alpha \times \beta \times \varphi^2)^{-1} \quad [2]$$

In this equation, ρ is the density of material, α is the pin shape factor, β is the shoulder shape factor, and the processing parameter $\varphi = \omega/v$. For the fixed welding parameters, *i.e.,* the same rotation rate, traveling speed, plunge depth, and welding tool, the M^{CR} is a constant. Generally, a FSW process without defect should meet the following inequality: $M^{PC} \geq M^{CR}$.

Let us focus on the role of the top Alclad layer first. As mentioned previously, the shoulder and pin drive the material to form the weld. Regular matching relations exist between size of the shoulder-driven zone and the pin-driven zone under different welding parameters. For the Unclad samples, a higher rotation rate tends to produce a larger shoulder-driven zone, a higher traveling speed tends to produce a larger pin-driven zone, and vice versa. The change in the welding parameters would cause the changes in the material flow patterns (Figure 4(b)). However, for the Alclad samples, there is always a soft Alclad layer at the tool/workpiece interface between shoulder and base material. It is noted that the shoulder (HV = 664) and the 2024Al-T351 base material (HV = 140) is much harder than the Alclad layer of pure aluminum (HV = 10 to 50). The soft Alclad layer plays a lubricating role during FSW. The plastic deformation of materials is driven by the friction between the shoulder and base material. Thus, the lubricating role of Alclad would reduce the friction coefficient, which changes the actual friction condition and weakens the plastic deformation of the material in the shoulder-driven zone. Therefore, the size of the shoulder-driven zone of the Alclad samples is much smaller than that of the Unclad samples, and a increase in the rotation rate usually could not enlarge the shoulder-driven zone. In this case, the variation in the welding parameters has no obvious influence on the material flow patterns of the shoulder-driven zone, but it influences the material flow patterns of the pin-driven zone only (Figure 4(a)), because the pin-driven zone is less affected by the shoulder.

Thus, the pin-driven material flow plays an important role during FSW. A low traveling speed would lead to a long stirring time per unit length and enough material flow from the shoulder-driven zone to the pin-driven zone, producing a sound FSW joint. An increase in the traveling speed shortens the stirring time per unit length, which reduces the material flow from the shoulder-driven zone to the pin-driven zone. On the one hand, the reduction in the material would lead to insufficient material fill to the hole at stage III. The void defects forms subsequently. On the other hand, an abnormal increase in the plunge depth could avoid the defects for the high-traveling-speed welds by increasing the material flowing to the pin-driven zone (Figures 1(d) and (e)). But a higher plunge depth would produce a higher temperature and a larger axial force,[23] which might lead to a transient local melting[24] and subsequently make the tool slippage easier at the tool/workpiece interface,[25] hence producing a unusual tool/workpiece slide. In this case, the rough weld surfaces were formed at stage IV (Figures 1(i) and (j)).

For the bottom Alclad layer, the distribution condition is controlled by the material flow of the swirl zone and excess material zone at stage II, which is related to the material flow state. The conception of material flow balance proposed by Arbegast[20] suggested that the three material flow states during FSW are insufficient material flow, balanced material flow, and excess material flow, which could be represented by following mass equations of flowing material, respectively:

$$M^{S} + M^{P} + M^{SW} + M^{EX} > \rho(\alpha \times \beta \times \varphi^2)^{-1} \quad (M^{EX} > 0) \quad [3]$$

$$M^{S} + M^{P} + M^{SW} + M^{EX} = \rho(\alpha \times \beta \times \varphi^2)^{-1} \quad (M^{EX} = 0) \quad [4]$$

$$M^{S} + M^{P} + M^{SW} + M^{EX} < \rho(\alpha \times \beta \times \varphi^2)^{-1} \quad (M^{EX} < 0) \quad [5]$$

Decreasing the traveling speed or increasing the rotation rate or plunge depth changed the material flow

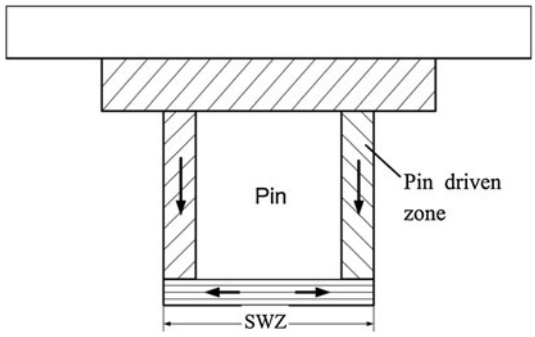

Fig. 9—Conceptual diagrams for role of bottom Alclad layer at stage II during insufficient and balanced material flow states.

state from insufficiency to balance and excess. Balanced material flow is the ideal welding state between insufficient and excess material flow states. For the three states, the material flow features are similar in stages I, III, and IV but different in stage II. Thus, stage II is the focus of discussion. At stage II, insufficient and balanced material flow states experience a similar process during which only the swirl zone forms (Figure 9). The swirl movement of the swirl zone makes the Alclad layer involve in the NZ evenly, which is the reason why there is no Alclad extending into the interior of the weld prepared at a high traveling speed and a small plunge depth (Figure 1(c)). Increasing the traveling speed, decreasing the rotation rate or the plunge depth would produce an excess material flow state with excess material zones (Figure 8(b)). The outward and upward movements of the excess material zone cause the Alclad layer extend into the weld along the boundaries of the NZ. Therefore, selecting the proper welding parameters of a high traveling speed or a small plunge depth to obtain a balanced material flow during FSW is the only way of avoiding the bottom Alclad extension. It is noted that the length of pin is another important parameter influencing the material flow at the swirl zone. A shorter pin (means a larger distance between the pin and bottom) tends to weaken the material flow of the swirl zone. But shortening in the length of a pin any more may lead to the root defect.

The Alclad layer thickness is another important influential factor for the Alclad samples. A thick Alclad layer, such as the current Alclad layer 0.2 mm in thickness, would cause the defects as mentioned previously. However, the harmful role of the Alclad layer would be reduced significantly when the Alclad layer is very thin; this concept needs additional investigation.

The discussion presented previously suggests strongly that the Alclad alloy has an optimum FSW condition, *i.e.*, a comparatively low traveling speed (or high rotation rate), a small plunge depth, and a proper length of pin, which could avoid the negative effect of the top and bottom Alclad layers on the FSW joints. Another study to minimize the excess material zone by adjusting the process parameters or the stirring tool is needed to obtain the perfect welds.

V. CONCLUSIONS

1. The shoulder dominates the material flow of the shoulder zone at the top. The top material flowed downward in the vertical direction on both advancing and retreating sides of the pin. The pin is responsible mainly for the pin-driven zone and swirl zone. For the material beneath the pin, a vertically swirl moment occurred.
2. The tool/workpiece interface plays a major role in determining the weld quality. For the Alclad samples, the soft top Alclad layer between the shoulder and workpiece changed the tool/workpiece interface condition and led to the void defects frequently at high traveling speeds.
3. The role of the bottom Alclad layer is related to the material flow states during FSW. Excess material flow led to the inward extension of the bottom Alclad layer, which was regarded as a defect and can be avoided at the balanced flow state.
4. Based on the experimental observations and the material flow characteristics during FSW, a comparatively low traveling speed (or high rotation rate), a small plunge depth and a proper pin length are the optimum welding condition to obtain a perfect weld for the Alclad 2024Al alloy.

ACKNOWLEDGMENTS

This work was supported by the National Outstanding Young Scientist Foundation of China under Grant 50525103 and the Hundred Talents Program of Chinese Academy of Sciences.

REFERENCES

1. D.Y. Jeong, O. Orringer, and G.C. Sih: *Theor. Appl. Fract. Mech.*, 1995, vol. 22, pp. 127–37.
2. D. Fersini and A. Pirondi: *Eng. Fract. Mech.*, 2007, vol. 74, pp. 468–80.
3. L. Commin, M. Dumont, J.E. Masse, and L. Barrallier: *Acta Mater.*, 2009, vol. 57, pp. 326–34.
4. R.S. Mishra and Z.Y. Ma: *Mater. Sci. Eng. R*, 2005, vol. 50R, pp. 1–78.
5. M.A. Sutton, B. Yang, A.P. Reynolds, and R. Taylor: *Mater. Sci. Eng. A.*, 2002, vol. 323, pp. 160–66.
6. C. Genevois, A. Deschamps, A. Denquin, and B. Doisneau-Cottignies: *Acta Mater.*, 2005, vol. 53, pp. 2447–58.
7. M.J. Jones, P. Heurtier, C. Desrayaud, F. Montheillet, D. Allehaux, and J.H. Driver: *Scripta Mater.*, 2005, vol. 52, pp. 693–97.
8. R. Talwar, D. Bolser, R. Lederich, and J. Baumann: *4th Int. Symp. Friction Stir Welding*, Park City, UT, 2003.
9. A.P. Reynolds: *Scripta Mater.*, 2008, vol. 58, pp. 338–42.
10. K. Colligan: *Weld J.*, 1999, vol. 78, pp. 229–37.
11. T.U. Seidel and A.P. Reynolds: *Metall. Mater. Trans. A*, 2001, vol. 32A, pp. 2879–84.
12. S.W. Xu and X.M. Deng: *Acta Mater.*, 2008, vol. 56, pp. 1326–41.
13. M. Guerra, C. Schmidt, J.C. McClure, L.E. Murr, and A.C. Nunes: *Mater. Charact.*, 2003, vol. 49, pp. 95–101.
14. H.N.B. Schmidt, T.L. Dickerson, and J.H. Hattel: *Acta Mater.*, 2006, vol. 54, pp. 1199–1209.
15. R.M. Leal, C. Leitao, A. Loureiro, D.M. Rodrigues, and P. Vilac: *Mater. Sci. Eng. A*, 2008, vol. 498, pp. 384–91.

16. O. Lorrain, V. Favier, H. Zahrouni, and D. Lawrjaniec: *J. Mater. Process. Tech.*, 2010, vol. 210, pp. 603–09.
17. K. Kumar and S.V. Kailas: *Mater. Sci. Eng. A.*, 2008, vol. 485, pp. 367–74.
18. H.W. Zhang, Z. Zhang, and J.T. Chen: *J. Mater. Res.*, 2007, vol. 183, pp. 62–70.
19. H. Schmidt and J. Hattel: *Proc. Symp. Friction Stir Welding Process. III*, TMS, Warrendale, PA, 2005, pp. 225 32.
20. W.J. Arbegast: *Scripta Mater.*, 2008, vol. 58, pp. 372–76.
21. Z.W. Chen, T. Pasang, and Y. Qi: *Mater. Sci. Eng. A*, 2008, vol. 474, pp. 312–16.
22. K. Kumar and S.V. Kailas: *Mater. Sci. Eng. A*, 2008, vol. 485, pp. 367–74.
23. S. Mandal, J. Rice, and A.A. Elmustafa: *J. Mater. Process. Tech.*, 2008, vol. 203, pp. 411–19.
24. A. Gerlich, M. Yamamoto, and T.H. North: *J. Mater. Sci.*, 2008, vol. 43, pp. 2–11.
25. A. Gerlich, G. Avramovic–Cingara, and T.H. North: *Metall. Mater. Trans. A*, 2006, vol. 37A, pp. 2773–86.